Soft Matter

PAPER

View Article Online
View Journal | View Issue

Cite this: *Soft Matter*, 2017, 13, 836

Emergence of collective dynamical chirality for achiral active particles†

Huijun Jiang, Huai Ding, Mingfeng Pu and Zhonghuai Hou*

Received 14th October 2016,
Accepted 21st December 2016

DOI: 10.1039/c6sm02335e

www.rsc.org/softmatter

Emergence of collective dynamical chirality (CDC) at mesoscopic scales plays a key role in many formation processes of chiral structures in nature, which may also provide possible routines for people to fabricate complex chiral architectures. So far, most of the reported CDCs have been found in systems of active objects with individual structure chirality or/and dynamical chirality, and whether CDC can arise from simple and achiral units is still an attractive mystery. Here, we report a spontaneous formation of CDC in a system of both dynamically and structurally achiral particles motivated by active motion of cells adhered onto a substrate. Active motion, confinement and hydrodynamic interaction are found to be the three key factors. Detailed analysis shows that the system can support abundant collective dynamical behaviors, including rotating droplets, rotating bubbles, CDC oscillations, arrays of collective rotations, and interesting transitions such as chirality transition, structure transition and state reentrance.

1 Introduction

Collective motion of natural or artificial micro(meso)scopic active objects has attracted growing research interest due to its ubiquity and importance in many systems.[1–6] One example is that groups of cells or their fragments can undergo active motion,[6–10] and a variety of fundamental processes in development, health and disease depend on such coordinated motions.[11–14] Since active systems can be driven far from equilibrium by continuously consuming energy supplied internally or externally, they are capable of completely altering the collective dynamical behaviors of interacting motile particles in a fashion that is forbidden for non-active particles.

Collective dynamical chirality (CDC) – mirror asymmetry of the collective motion of motile objects – is one of such interesting behaviors supported in active systems. On the one hand, CDC plays a crucial role in many processes in nature. For instance, establishment of left–right asymmetry in embryonic development, one of the most intriguing biological phenomena, involves coordinated activity of many cells[15,16] where the ability of the cells to distinguish between the left and the right is evident in systems of chiral patterns formed by collective motion of identical cells confined in circular island or ring/stripe-shaped micropatterns.[17–20] On the other hand, CDC may also inspire new routines for fabrication of complex chiral architectures by dynamically self-assembling simple and achiral building blocks,[21] *e.g.*, chiral clusters of asymmetric colloidal dimers have been successfully assembled by using alternating current electric fields.[22] Revealing how CDC arises from groups of active units is then very important for the understanding of the formation mechanism.

So far, CDC can be found in systems of active objects with individual structure chirality and/or individual dynamical chirality. For example, CDC has been reported in several experiments where vortexes were observed for microtubules,[23] actin filaments,[24,25] or sperm cells[26] moving on a planar surface. It is believed that individual dynamical chirality might be caused by the rotation of the microtubule around its axis[27] or by the special slender shape,[28] while interactions between active objects help to align their moving direction.[23,26,29] Besides, man-made catalytical nanorods,[30,31] self-motile colloids[32] or rotating disks[5] can also be dynamically chiral in the form of swimming in circles, and hydrodynamic interaction can synchronize them to form CDC.[5] There is also a recent study of elliptical active particles where particles can rotate in a circular confinement.[4] For structurally chiral objects, dynamical chirality will arise when they are driven by external fields through potential landscapes, and CDC can provide an efficient method for chirality sorting.[33–36] Very recently, a metastable CDC is reported in a system with achiral interaction.[37] Since such a metastable chiral state will relax to a more stable state for a finite temperature, whether stable CDC can emerge in systems of simple particles without both individual structure chirality and dynamical chirality is still a very attractive mystery.

In this paper, we employ a model motivated by active motion of cells adhered onto a surface in a fluid environment to address

Department of Chemical Physics & Hefei National Laboratory for Physical Sciences at Microscales, iChEM, University of Science and Technology of China, Hefei, Anhui 230026, China. E-mail: hzhlj@ustc.edu.cn

† Electronic supplementary information (ESI) available: Simulation details of the lattice Boltzmann method. See DOI: 10.1039/c6sm02335e

such a question. The model consists of three elementary ingredients, *i.e.*, achiral active motion, confined space for particle motion and hydrodynamic interaction (HI) between particles, to avoid other complexities such as special shape or structure chirality in real systems which perplexes us to understand the fundamental mechanism underlying the formation of CDC.[21] Remarkably, we find that CDC emerges spontaneously in the form of collective rotation for active forces larger than a critical value, near which an interesting oscillation between clockwise and anti-clockwise rotation is observed. Detailed analysis reveals that confinement and HI, along with the active motion of particles, are sufficient for the formation of CDC, while other details such as confinement shape and boundary conditions are not relevant. Moreover, the phase diagram shows that the system supports abundant collective states, *e.g.*, two distinct states of CDC, a rotating droplet state and a rotating bubble state, are identified by a structure transition of CDC states, and interesting transition behaviors such as state reentrance from the fluid-like state to a rotating droplet then back to the fluid-like state can also be observed. In addition, we find that the number of collective rotations is determined by the length/width ratio of the confinement: a single droplet can be found in squares, while arrays of multiple droplets are observed in rectangles.

2 Model

We consider a system consisting of N active spherical particles moving in a two-dimensional rectangular confined space of size $L \times W$, where L and W are the length and the width, respectively. Active motion of particles is realized by exerting a constant force (f_0) along the internal active directions, which mimics movement of cells adhered onto a surface.[7] The only direct interaction between particles is an exclusive volume effect taken into account by a Weeks–Chandler–Andersen potential, $U(\mathbf{r}_{ij}) = 4\varepsilon\{(2a/r_{ij})^{12} - (2a/r_{ij})^{6}\} + \varepsilon$ existing only if $r_{ij} < 2\sqrt[6]{2}a$, where a is the effective repulsion radius, $\mathbf{r}_i$ the position of particle i, and r_{ij} the distance between the i-th and j-th particles. Particles can also interact with each other indirectly by long-range HI through the ambient fluid, where the force on the i-th particle generated by the fluid is $\mathbf{F}_{i,\mathrm{fl}} = -\gamma[\dot{\mathbf{r}}_i - \mathbf{u}(\mathbf{r}_i, t)]$ with γ the friction coefficient and $\mathbf{u}(\mathbf{r}_i, t)$ the fluid velocity at location $\mathbf{r}_i$. In our work, $\mathbf{u}(\mathbf{r}_i, t)$ is calculated by using a stochastic lattice Boltzmann method where particles are treated as point-like objects.[38] Simulation details of the lattice Boltzmann method can be found in the ESI.† The equations for translational motion of particles with mass m are then

$$m\ddot{\mathbf{r}}_i = f_0\mathbf{n}_i + \mathbf{F}_{i,\mathrm{fl}} - \sum_{j=1}^{N}\frac{\partial U(\mathbf{r}_{ij})}{\partial \mathbf{r}_{ij}} + \xi_i,\ i = 1, \ldots, N. \quad (1)$$

Herein, $\xi_i(t)$ denotes the fluctuation force satisfying the fluctuation–dissipation relationship $\langle\xi_i(t)\xi_j(t')\rangle = 2\gamma k_{\mathrm{B}}T\delta(t - t')\delta_{ij}$, where k_{B} is the Boltzmann constant, T denotes the temperature, and $\mathbf{n}_i = (\cos\theta_i, \sin\theta_i)$ is the direction of the active force. Besides, the angle θ_i is steered towards the direction of the total force on the i-th particle by the rule similar to that in ref. 6 and 39

$$\dot{\theta}_i = (1/\tau)[\arg(\ddot{\mathbf{r}}_i) - \theta_i] + \zeta_i \quad (2)$$

where $\arg(\ddot{\mathbf{r}}_i)$ is the angle of the total force vector, and $\zeta_i(t)$ is the rotational fluctuation satisfying $\langle\zeta_i(t)\zeta_j(t')\rangle = 3k_{\mathrm{B}}T\delta(t - t')\delta_{ij}/(2a^2\gamma)$. Such a steering rule is motivated by the fact that cells can respond to mechanical forces,[10,40,41] which is also consistent with reported positive feedback regulation of front-rear cell polarity by actual cell displacements.[42,43] The resistance time τ for active orientation measures the ability of particles resisting such external steering. For a small τ, active particles will yield to the steering very fast, while for a large enough τ they tend to keep their internal random behavior similar to the conventional ones without the steering rule.[44,45] We rescale the density, time and length by the particle density, the simulation time step of the lattice Boltzmann method, and the grid length of the lattice, respectively. We fix $k_{\mathrm{B}}T = 10^{-7}$, $\varepsilon = 5 \times 10^{-4}$, $a = 0.75$, and $\gamma = (32/3)a\nu\rho$ with fluid viscosity $\nu = 0.1$ and density $\rho = 1$, for which the system will reach a fluid-like state in the absence of active force. The resistance time, active force, number of particles and size of the space are $\tau = 1$, $f_0 = 1.25 \times 10^{-5}$, $N = 2500$ and $L = W = 100$ (corresponding to a volume fraction of about 0.442), if not otherwise stated. The interaction between active particles and the confined boundary is realized by the bounce-back rule.

3 Results

To begin with, we investigate how the collective motion of particles depends on the magnitude f_0 of the active force. For a small active force, *e.g.*, $f_0 = 8 \times 10^{-7}$, the system is still fluid-like where particles move randomly. Quite interestingly, a CDC state emerges spontaneously if the active force becomes large enough. A typical snapshot of such a state for $f_0 = 1.25 \times 10^{-5}$ is presented in Fig. 1(a) where all the particles rotate collectively around the center of the space $\mathbf{r}_{\mathrm{c}} = (L/2, W/2)$. To quantitatively characterize the CDC of the system, we define an order parameter

$$q = \frac{1}{N}\sum_{i=1}^{N}\varphi_i. \quad (3)$$

Here, $\varphi_i = \omega_i/|\omega_i|$ denotes the "dynamical-chirality spin" of particle i, where $\omega_i = (\mathbf{r}_i - \mathbf{r}_{\mathrm{c}}) \times \dot{\mathbf{r}}_i/|(\mathbf{r}_i - \mathbf{r}_{\mathrm{c}})|^2$ is the angular velocity of the i-th particle relative to $\mathbf{r}_{\mathrm{c}}$. Note that φ_i is equal to 1 for anti-clockwise rotation and -1 for clockwise rotation. Time-dependencies of q for $f_0 = 8 \times 10^{-7}$ and 1.25×10^{-5} are plotted in Fig. 1(b). It can be observed that q fluctuates around a fixed value after a quick relaxation, indicating that the system can finally reach a stable steady state. Time-averaged q equals 0 for the fluid-like state, and is of a negative (or positive) value for the CDC state with collective clockwise (or anti-clockwise) rotation.

To obtain a global picture for how CDC emerges as f_0 increases, the magnitude of time-averaged q,

$$Q = \left|\lim_{t_0\to\infty}\frac{1}{t_0}\int_0^{t_0} q(t)\mathrm{d}t\right| \quad (4)$$

as a function of f_0 is drawn in Fig. 1(c). For spherical active particles, there is also another parameter to measure the activity of particles, *i.e.*, the Péclet number $\mathrm{Pe} = |f_0|a/(k_{\mathrm{B}}T)$.

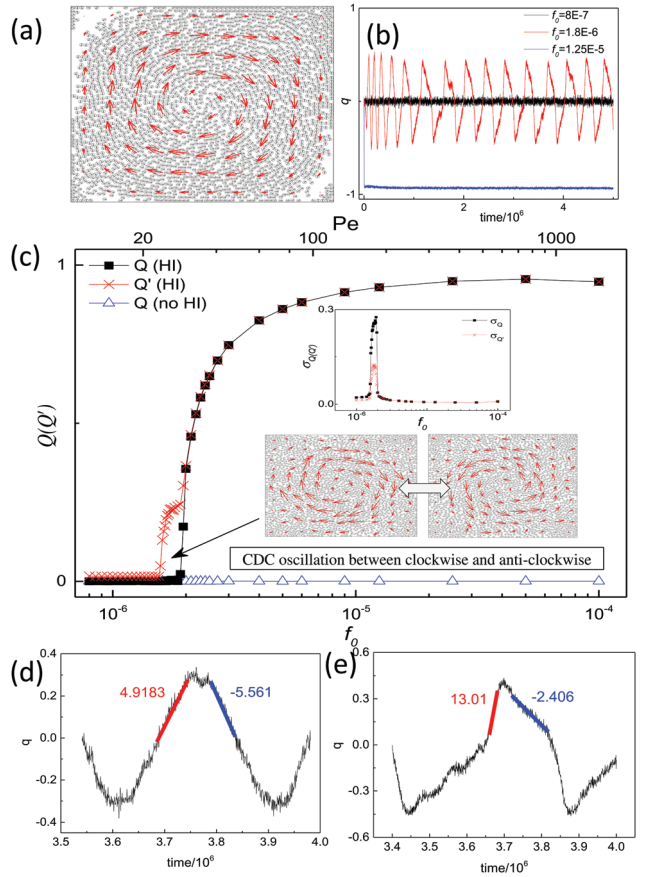

Fig. 1 Spontaneous emergence of collective dynamical chirality. (a) Typical snapshot of the CDC state for $f_0 = 1.25 \times 10^{-5}$. Red arrows are locally averaged velocities of particles in the nearest 10 × 10 grids (normalized by the maximal velocity). (b) Time series of q for $f_0 = 8 \times 10^{-7}$, 1.8×10^{-6} and 1.25×10^{-5}. (c) Dependence of order parameters Q and Q' on the active force f_0. The standard deviation of Q is plotted in the top inset and typical snapshots of clockwise and anti-clockwise rotation during chirality oscillation in the bottom. For comparison, Q without hydrodynamic interaction and its standard deviation are also plotted. For (d) $f_0 = 1.67 \times 10^{-6}$ and (e) $f_0 = 1.8 \times 10^{-6}$, time scales for the onset of CDC away from $q = 0$ and the decay towards $q = 0$ are shown by slopes of red and blue lines, respectively.

For comparison, the corresponding value of Pe is also shown in the top axis in Fig. 1(c). Clearly, a continuous-like transition from the fluid-like state to a CDC state induced by particle activity is observed: Q is nearly zero for small forces and quickly increases to be nearly 1 for f_0 larger than the threshold $f_c \simeq 1.9 \times 10^{-6}$. By defining the standard deviation as $\sigma_Q = \sqrt{(1/t_0)\int_0^{t_0}[q(t) - \bar{q}]^2 \mathrm{d}t}$, where $\bar{q}$ is the mean value of $q(t)$, σ_Q exhibits a clear-cut peak as shown in the top inset of Fig. 1(c). The presence of f_c may be understood by the following observations. By taking a close look at the top-right and bottom-left corner in Fig. 1(a), it can be seen that collective rotation can lead to accumulation of particles near the boundary at those corners. The accumulation will in return provide an obstacle for particles to rotate collectively and consequently an effective barrier for emergence of CDC.

Remarkably, we also observe an interesting oscillation of CDC. As depicted in Fig. 1(b), particles rotate periodically between clockwise and anti-clockwise for an active force slightly smaller than f_c, *e.g.*, $f_0 = 1.8 \times 10^{-6}$, whose typical snapshots are shown in the bottom-left and bottom-right insets of Fig. 1(c). The formation of CDC oscillation may be due to competition of the onset process of CDC away from $q = 0$ and the decay process towards $q = 0$. In Fig. 1(d), rates of these two processes are presented by absolute values of the time-series slope for $f_0 = 1.67 \times 10^{-6}$, where the onset rate is about 4.92 while the decay rate is 5.56. When the active force f_0 approaches the threshold f_c, for example $f_0 = 1.8 \times 10^{-6}$, the onset process is accelerated to be of a slope 13.1; meanwhile, the decay rate decreases to 2.406 (Fig. 1(e)). The observation implies that CDC is hard to onset and easy to decay for small active forces, and the decay rate may approach 0 and only emergence of CDC can be observed for large enough active forces. Thus, an appropriate active force can lead to CDC oscillation. To elucidate more clearly the detailed mechanism for the formation of CDC oscillation, a follow-up study may be needed.

To identify the region of CDC oscillation, the time-averaged magnitude of q, $Q' = \lim_{t_0 \to \infty}(1/t_0)\int_0^{t_0}|q(t)|\mathrm{d}t$, is presented in Fig. 1(c). It can be found that Q' is overlapped with Q very well for small or large active forces. In the CDC region where active force is in the range $1.55 \times 10^{-6} < f_0 < f_c$, $Q = 0$ indicates that there is no time-averaged CDC, while Q' is larger than zero obviously, demonstrating that particles do rotate collectively for a given time. The standard deviation of Q', $\sigma_{Q'} = \sqrt{(1/t_0)\int_0^{t_0}[|q(t)| - |\bar{q}|]^2 \mathrm{d}t}$, where $|\bar{q}|$ is the mean value of $|q(t)|$, is also plotted in the top inset of Fig. 1(c), which shows a peak at $f_0 \simeq 1.9 \times 10^{-6}$ as same as that of Q, demonstrating that chirality oscillation is not a new dynamical phase of the system.

One may be wondering what are the key ingredients that lead to the above interesting observations. In fact, we find that besides active motion, the long range HI and space confinement are two other necessary conditions for emergence of CDC as well as the CDC-oscillation. To show this, we have performed parallel simulations with the same parameter settings as above but with the HI turned off by using Brownian dynamics where the diffusion coefficient of a free-diffusion particle is ensured to be the same. The obtained Q without HI is plotted in Fig. 1(c) to be compared with the one with HI. Clearly, there is no CDC that can be observed for all ranges of parameters. We also repeat similar simulations for collective motion of particles without confinement, and no CDC is found, too. What's more, other rules of interaction between active particles and the confined boundary such as the reflecting rule are also tested, and our findings are not sensitive to the boundary conditions. In short, HI and confinement, along with activity of particles, are the three key factors for the emergence of CDC. Note that active particles we used here are force monopoles to mimic movement of cells adhered onto a surface. For microswimmers suspended in a fluid, they form at least force dipoles. We have repeated similar simulations for microswimmers, and no CDC was observed for the parameters presented here.

It is noted that the dynamics of active particles may change dramatically for different resistance times for the active

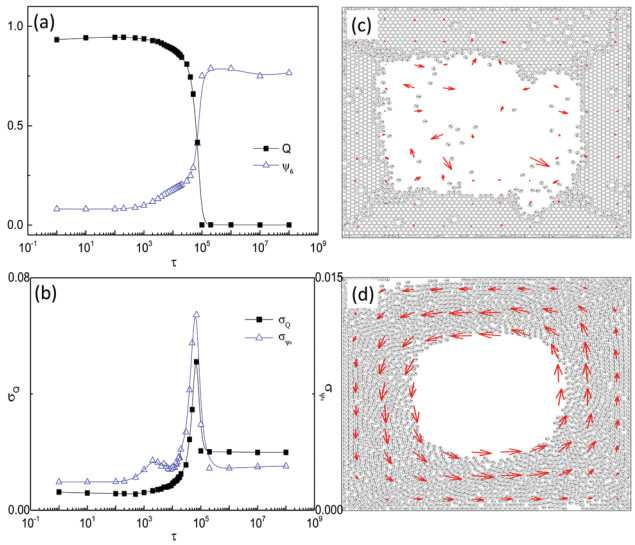

Fig. 2 (a) Dependence of order parameters Q and Ψ_6 on resistance time τ. (b) Standard deviation of order parameters as functions of τ. (c) Typical snapshots of the crystal-like state for $\tau = 10^8$ and (d) the rotating bubble state for $\tau = 10^4$. The locally averaged velocities of particles normalized by the maximal velocity are presented by red arrows.

direction; thus, we now try to figure out how τ affects collective motion of active particles. In Fig. 2(a), Q as a function of τ is plotted by fixing $f_0 = 1.25 \times 10^{-5}$, where a transition between a CDC and an achiral state can also be found. A typical snapshot of the achiral state is presented in Fig. 2(c). Different from the fluid-like state, the achiral state observed here is crystal-like where particles are arranged in hexagonal order. The ordering can be measured by[46]

$$\Psi_6 = \frac{1}{N}\sum_{m=1}^{N}\frac{1}{N_m}\sum_{l=1}^{N_m}\exp(6i\theta_{ml}), \qquad (5)$$

where i is the imaginary unit, θ_{ml} is the angle between an arbitrary reference axis and the displacement vector between particles m and l, and the sum runs over the nearest $N_m = 6$ particles within a cutoff radius of $2.6a$ from particle m (for particles adjacent to the confined boundary, only $N_m = 4$ neighbors are needed to form hexagonal ordering). In Fig. 2(a), Ψ_6 increases from a value near 0 to about 1 as τ increases, indicating a structure transition from the CDC state to the crystal-like state when collective motion of particles changes.

If one takes a closer look at the dependence of Ψ_6 on τ, it can be found that there seems to be a shoulder before the transition occurs. For more detailed information, standard deviations σ of Q and Ψ_6 are given in Fig. 2(b). As expected, peaks are observed for both σ_Q and σ_{Ψ_6} at $\tau_c \simeq 7 \times 10^4$, corresponding to the transition of both chirality and structure from the CDC state to the crystal-like state. It is quite interesting that there is also another peak of σ_{Ψ_6} at $\tau_s \simeq 2 \times 10^3$ where no peaks of σ_Q are found, *i.e.*, the CDC state undergoes a structure transition without loss of chirality. By comparison between the snapshot for $\tau = 1 < \tau_s$ in Fig. 1(b) and a typical snapshot presented in Fig. 2(d) for $\tau_s < \tau = 10^4 < \tau_c$, we can mark these two states of CDC as a rotating droplet for the former and a rotating bubble for the latter.

In order to explore fully how parameters affect particles' collective motion, a phase diagram in the f_0–τ plane is obtained by extensive simulations (Fig. 3(a)). Several interesting remarks can be made. Firstly, there is a triple-point-like point located at (f_{tp}, τ_{tp}) where the CDC state meets both fluid-like and crystal-like states. For $\tau < \tau_{tp}$, CDC can arise spontaneously, while for larger τ only a fluid-like state and a crystal-like state can be observed. Note that the steering rule in eqn (2) can be neglected for large enough τ; the observation is in good agreement with findings reported in the literature.[44,45] Secondly, structure transition between the two states of CDC, the rotating droplet and the rotating bubble, occurs only for $f_0 > f_{tp}$, below which the rotating droplet is the sole CDC state. Lastly, the system can also support other interesting state transition behaviors. As indicated by the gray arrow in Fig. 3, a state reentrance can be found as τ increases for $f_0 < f_{tp}$, *i.e.*, particles are first fluid-like for small τ, then change to be of CDC for intermediate τ, then back to be fluid-like when τ is large enough. The corresponding color plot for Q and the contour plot for Ψ_6 are also presented in Fig. 3(b). It can be found that, as τ passes by τ_{tp}, transition from the fluid/crystalline to the chiral state results in a rapid increase in Q for large f_0 as already shown in Fig. 2. Moreover, for small f_0 the change is much more subdued, indicating that the two fluid-like areas are connected for very small f_0. When f_0 crosses f_{tp}, *i.e.* the system goes from the fluid to the crystalline state, we see that the Ψ_6 increases rapidly, showing a crystallisation/melting transition due to activity. Furthermore, the rotating bubble has

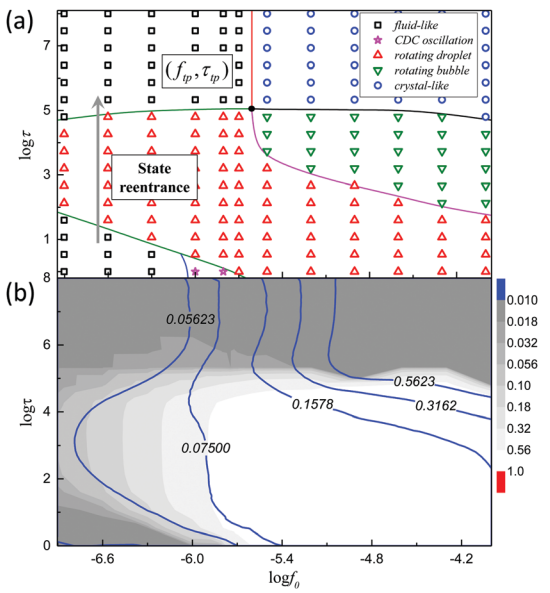

Fig. 3 (a) Phase diagram on the f_0–τ plane. There is a triple-point-like point (f_{tp}, τ_{tp}) above which no CDC can be formed for $\tau > \tau_{tp}$, and a state reentrance from the fluid-like state to a rotating droplet state then back to the fluid-like state can be found as indicated by the gray arrow. (b) The color plot for Q and the contour plot for Ψ_6 in the same parameter region as in (a). The color from gray to white indicates the value of Q from 0.01 to 1 and lines with labels present the corresponding values of Ψ_6.

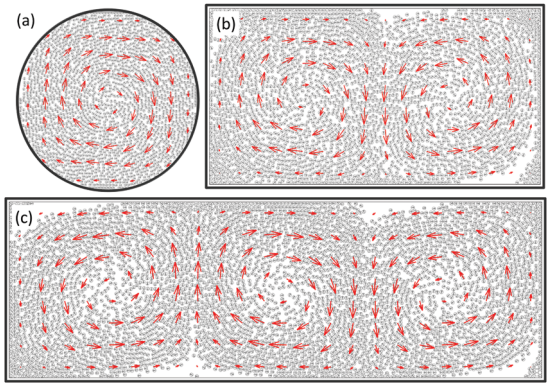

Fig. 4 Collective dynamical chirality for different boundary shapes. (a) Circle with a diameter of 100, and rectangles with (b) 160 × 80 and (c) 240 × 80 for $f_0 = 1.25 \times 10^{-5}$ and $\tau = 1$.

a higher Ψ_6 than the rotating droplet, which is probably due to the walls facilitating a hexagonal order.

At last, effects of the confinement shape on CDC are also considered. A typical snapshot for collective motion of particles in a circular confined space with a diameter of 100 is shown in Fig. 4(a). Similarly, CDC emerges for the same parameters as in the square space, indicating that formation of CDC is not sensitive to the confinement shape. The dynamics of particles in confinement with different length/width ratios are also investigated. Typical snapshots for $L \times W = 160 \times 80$ and 240×80 are presented in Fig. 4(b) and (c), respectively, where the number of particles is set to be $N = 3200$ for the former and $N = 4800$ for the latter to keep the volume fraction unchanged. Interestingly, an array of vortexes with opposite chirality for adjacent ones is observed, and the number of vortexes seems to be proportional to the length/width ratio.

4 Conclusions

In summary, it was revealed that active motion, space confinement and hydrodynamic interaction are sufficient for the emergence of CDC in a system of active particles without individual structure chirality and dynamical chirality. CDC states were found to be formed *via* a chirality transition from other achiral states such as a fluid-like state or a crystal-like state, while they can also undergo a structure transition to form two distinct states, *i.e.*, a rotating droplet and a rotating bubble. The phase diagram showed that CDC formation is controlled by the active force and the resistance time for particles to maintain their internal motion. More interestingly, CDC oscillation can also be supported by the system. Formation of CDC oscillation may be due to a competition between the onset process of CDC away from $q = 0$ and the decay process towards $q = 0$. Since the emergence of CDC underlies many formation processes of chiral structures, our finding may inspire experimental studies to explore new routines for fabrication of complex chiral architectures from simple and achiral units, and shed light on the understanding of chirality formation in other complex systems such as establishment of left–right asymmetry in embryonic development.

Acknowledgements

This work was supported by the National Basic Research Program of China (Grant No. 2013CB834606), the National Science Foundation of China (Grant No. 21673212, 21521001, 21473165, and 21403204), the Ministry of Science and Technology of China (Grant No. 2016YFA0400904), and the Fundamental Research Funds for the Central Universities (Grant No. WK2060030018, 2030020028, and 2340000074).

References

1 M. Marchetti, J. F. Joanny, S. Ramaswamy, T. B. Liverpool, J. Prost, M. Rao and R. A. Simha, *Rev. Mod. Phys.*, 2013, **85**, 1143.
2 J. Elgeti, R. G. Winkler and G. Gompper, *Rep. Prog. Phys.*, 2015, **78**, 056601.
3 H. Wioland, F. G. Woodhouse, J. Dunkel and R. E. Goldstein, *Nat. Phys.*, 2016, **12**, 341.
4 E. Lushi, H. Wioland and R. E. Goldstein, *Proc. Natl. Acad. Sci. U. S. A.*, 2014, **111**, 9733.
5 Y. Goto and H. Tanaka, *Nat. Commun.*, 2015, **6**, 5994.
6 B. Szabo, G. J. Szöllösi, B. Gönci, Z. Jurányi, D. Selmeczi and T. Vicsek, *Phys. Rev. E: Stat., Nonlinear, Soft Matter Phys.*, 2006, **74**, 061908.
7 R. Ananthakrishnan and A. Ehrlicher, *Int. J. Biol. Sci.*, 2007, **3**, 303.
8 G. F. Weber, M. A. Bjerke and D. W. DeSimone, *Dev. Cell*, 2012, **22**, 104.
9 K. Sato, T. Hiraiwa and T. Shibata, *Phys. Rev. Lett.*, 2015, **115**, 188102.
10 D. T. Tambe, C. C. Hardin, T. E. Angelini, K. Rajendran, C. Y. Park, X. Serr-Picamal, E. H. Zhou, M. H. Zaman, J. P. Butler and D. A. Weitz, et al., *Nat. Mater.*, 2011, **10**, 469.
11 K. R. Levental, H. Yu, L. Kass, J. N. Lakins, M. Egeblad, J. T. Erler, S. F. Fong, K. Csiszar, A. Giaccia and W. Weninger, et al., *Cell*, 2009, **139**, 891.
12 A. Bianco, M. Poukkula, A. Cliffe, J. Mathieu, C. M. Luque, T. A. Fulga and P. Rørth, *Nature*, 2007, **448**, 362.
13 P. Friedl and D. Gilmour, *Nat. Rev. Mol. Cell Biol.*, 2009, **10**, 445.
14 D. J. Montell, *Science*, 2008, **322**, 1502.
15 M. Blum, K. Feistel, T. Thumberger and A. Schweickert, *Development*, 2014, **141**, 1603.
16 J.-B. Coutelis, N. González-Morales, C. Géminard and S. Noselli, *EMBO reports*, 2014, p. e201438972.
17 L. Q. Wan, K. Ronaldson, M. Park, G. Taylor, Y. Zhang, J. M. Gimble and G. Vunjak-Novakovic, *Proc. Natl. Acad. Sci. U. S. A.*, 2011, **108**, 12295.
18 H. Yamanaka and S. Kondo, *Genes Cells*, 2015, **20**, 29.
19 A. Tamada, S. Kawase, F. Murakami and H. Kamiguchi, *J. Cell Biol.*, 2010, **188**, 429.
20 J. Xu, A. Van Keymeulen, N. M. Wakida, P. Carlton, M. W. Berns and H. R. Bourne, *Proc. Natl. Acad. Sci. U. S. A.*, 2007, **104**, 9296.
21 A. Guerrero-Martnez, J. L. Alonso-Gómez, B. Auguié, M. M. Cid and L. M. Liz-Marzán, *Nano Today*, 2011, **6**, 381.
22 F. Ma, S. Wang, D. T. Wu and N. Wu, *Proc. Natl. Acad. Sci. U. S. A.*, 2015, **112**, 6307.

23 Y. Sumino, K. H. Nagai, Y. Shitaka, D. Tanaka, K. Yoshikawa, H. Chaté and K. Oiwa, *Nature*, 2012, **483**, 448.
24 F. G. Woodhouse and R. E. Goldstein, *Phys. Rev. Lett.*, 2012, **109**, 168105.
25 V. Schaller, C. Weber, C. Semmrich, E. Frey and A. R. Bausch, *Nature*, 2010, **467**, 73.
26 I. H. Riedel, K. Kruse and J. Howard, *Science*, 2005, **309**, 300.
27 O. Kagami and R. Kamiya, *J. Cell Sci.*, 1992, **103**, 653.
28 H. Jiang and Z. Hou, *Soft Matter*, 2014, **10**, 1012.
29 H. Jiang and Z. Hou, *Soft Matter*, 2014, **10**, 9248.
30 P. Dhar, T. M. Fischer, Y. Wang, T. Mallouk, W. Paxton and A. Sen, *Nano Lett.*, 2006, **6**, 66.
31 L. Qin, M. J. Banholzer, X. Xu, L. Huang and C. A. Mirkin, *J. Am. Chem. Soc.*, 2007, **129**, 14870.
32 J. Gibbs, S. Kothari, D. Saintillan and Y.-P. Zhao, *Nano Lett.*, 2011, **11**, 2543.
33 M. Kostur, M. Schindler, P. Talkner and P. Hänggi, *Phys. Rev. Lett.*, 2006, **96**, 014502.
34 D. Speer, R. Eichhorn and P. Reimann, *Phys. Rev. Lett.*, 2010, **105**, 090602.
35 L. Bogunovic, M. Fliedner, R. Eichhorn, S. Wegener, J. Regtmeier, D. Anselmetti and P. Reimann, *Phys. Rev. Lett.*, 2012, **109**, 100603.
36 A. Nourhani, V. H. Crespi and P. E. Lammert, *Phys. Rev. Lett.*, 2015, **115**, 118101.
37 R. E. Breier, R. L. B. Selinger, G. Ciccotti, S. Herminghaus and M. G. Mazza, *Phys. Rev. E*, 2016, **93**, 022410.
38 P. Ahlrichs and B. Dünweg, *Int. J. Mod. Phys. C*, 1998, **9**, 1429.
39 E. Mones, A. Czirók and T. Vicsek, *New J. Phys.*, 2015, **17**, 063013.
40 M. M. Kozlov and A. Mogilner, *Biophys. J.*, 2007, **93**, 3811.
41 P. T. Yam, C. A. Wilson, L. Ji, B. Hebert, E. L. Barnhart, N. A. Dye, P. W. Wiseman, G. Danuser and J. A. Theriot, *J. Cell Biol.*, 2007, **178**, 1207.
42 A. T. Dawes and L. Edelstein-Keshet, *Biophys. J.*, 2007, **92**, 744.
43 A. Szabó, R. Ünnep, E. Méhes, W. Twal, W. Argraves, Y. Cao and A. Czirók, *Phys. Biol.*, 2010, **7**, 046007.
44 T. Speck, J. Bialké, A. M. Menzel and H. Löwen, *Phys. Rev. Lett.*, 2014, **112**, 218304.
45 R. Ni, M. A. C. Stuart and P. G. Bolhuis, *Phys. Rev. Lett.*, 2015, **114**, 018302.
46 J. Stenhammar, R. Wittkowski, D. Marenduzzo and M. E. Cates, *Phys. Rev. Lett.*, 2015, **114**, 018301.